Impact of phase evolution in Platreef and UG-2 concentrates on matte drainage in the black top of a platinum group metal smelter

Oscar Rivera[a] and Andrie Garbers-Craig [a*]

[a] Centre for Pyrometallurgy, Department of Materials Science and Metallurgical Engineering, University of Pretoria, Private Bag X20, Hatfield 0028

* Corresponding author: andrie.garbers-craig@up.ac.za

Abstract

The melting behaviour of Platreef and UG–2 platinum group metal (PGM) concentrates was studied under conditions typically found in the black top of PGM smelters. In order to understand how the phase changes influence the separation between matte and slag, the concentrates were characterised before and after firing at eight temperatures from 800 to 1480 °C. The PGM concentrates were isothermally heated in either silica (Platreef) or magnesia crucibles (UG–2), which in turn were sealed in steel capsules under argon atmosphere. This configuration prevented the escape of sulphur–containing gases during the experiments. Observed phase relations were compared against phase relations predicted by FactSage® under oxygen partial pressures in the range of 10^{-18} to 10^{-9} bar and sulphur partial pressures in the range of 10^{-9} to $10^{-3.5}$ bar. The results showed the effective separation of matte from the gangue minerals at sub–liquidus temperatures of the gangue (1480 °C for UG–2 concentrate, 1400 and 1480 °C for Platreef concentrate). The PGM concentrates did not sinter at low temperatures (800 – 1100 °C); however, from 1200 °C the formation of a liquid phase promoted liquid phase sintering. The collection of matte in a button at the bottom of the crucible was facilitated by the formation of a continuous liquid phase in the sintered concentrate, through which the matte droplets could descend. This occurred after the main gangue phase, enstatite, melted incongruently.

Keywords: Platinum group metals; black top; smelting; concentrate; enstatite; matte separation

Introduction

Platinum group metals (PGMs) consist of a group of six elements: platinum (Pt), palladium (Pd), rhodium (Rh), iridium (Ir), osmium (Os) and ruthenium (Ru). These elements have high resistances to oxidation and corrosion, high electrical conductivities and superior catalytic properties. Because of these unique properties, PGMs are in strong demand in the automotive, jewellery, chemical, petroleum, dental, glass and investment industries (Jones, 2005; Sahu et al., 2020).

South Africa is the world leader in PGM production with 69% and 13% of the total world mine production of Pt and Pd, respectively. Russia is the second largest PGM producer, as by–product of nickel mining, with 13% and 40% of the world mine production of Pt and Pd, respectively (Singerling, 2019). In South Africa, the PGM–containing ore is concentrated through comminution and froth flotation, after which it is smelted, converted and refined in order to recover the individual base metals Cu, Ni and Co as well as the PGMs (Crundwell, 2011).

PGM concentrates consist of sulphide phases and oxide gangue which during smelting separate from each other in a slag layer and a PGM–containing matte layer. In the smelting process the unsmelted concentrate layer, called the black top (BT), floats on top of the molten slag bath and thereby protects the refractories in the sidewall and roof from thermal radiation (Jones, 2005). The permeability of the BT influences matte drainage through this layer as sintering of the gangue matrix can potentially occlude and immobilise the descending liquid matte droplets, decreasing or even stopping matte drainage. Unlike in the copper and nickel industries, the sulphides content in the PGM concentrates is low – sometimes less than 15 mass%. Autothermal smelting (flash smelting) is therefore not feasible in the PGM industry. The presence of magnesium and

chromium oxides in the PGM concentrates also increase the liquidus temperatures of the produced slag to temperatures of 1600 – 1700 °C (Nell, 2004).

The mechanism by which matte moves through the BT, before it passes through the slag and finally collects in the hearth of the smelter has been a topic of discussion for many years. Two possibilities were hypothesised: The first was that matte, which has a liquidus temperature below 1000°C, can trickle through the porosity of a solid sintered gangue layer, pass through the slag layer and collect in the hearth; while the second possibility is that gangue must be fully molten before matte can separate from it and collect in a separate matte layer. This paper therefore describes the first comprehensive laboratory study on phase evolution and melting behaviour of gangue minerals in the BT, and how it impacts on matte drainage in the PGM smelter. This was done on a laboratory scale by reacting concentrate samples from 800°C (simulating conditions in the freeboard) to 1480°C (simulating conditions at the BT – molten slag interface).

Background

South African PGM-containing ores consist of a mixture of silicate and oxide-based gangue minerals together with the sulphides pentlandite ($(Fe,Ni)_9S_8$), chalcopyrite ($CuFeS_2$), pyrrhotite ($Fe_{1-x}S$) and pyrite (FeS_2) (Schouwstra et al., 2000; Sinisalo & Lundström, 2018). The main gangue minerals are pyroxenes ($(Ca,Mg,Fe)_2Si_2O_6$), plagioclase feldspar ($NaAlSi_3O_8$–$CaAl_2Si_2O_8$) and phlogopite ($KMg_3(AlSi_3)O_{10}(OH)_2$) in the Merensky Reef, chromite ($(Mg,Fe^{2+})(Cr,Mg,Al,Fe^{3+})_2O_4$), pyroxenes and plagioclase feldspar in the UG-2 Reef and pyroxenes, olivine ($(Mg,Fe)_2SiO_4$), serpentine ($(Mg,Fe)_3Si_2O_5(OH)_4$) and calc-silicates (lime-rich minerals) in the Platreef Reef. Secondary minerals include talc ($Mg_3Si_4O_{10}(OH)_2$), chlorite

($(Mg,Fe)_5Al(Si_3Al)O_{10}(OH)_8$), biotite ($K(Mg,Fe^{2+})_3(Al,Fe^{3+})Si_3O_{10}(OH, F)_2$) and magnetite ($Fe_3O_4$) (Schouwstra et al., 2000). The gangue minerals comprise over 80% of the crystalline phases in the PGM concentrate. The most relevant transformations associated with the gangue minerals on heating are vaporisation of absorbed water; dehydroxylation, i.e. releasing of structural molecular water (Ewell et al., 1935) and solid–state reactions and melting (Belgacem et al., 2008; F. Crundwell, 2011; Eksteen, 2011). Since South African PGM concentrates contain compounds such as plagioclase feldspar, phlogopite and biotite, potassium and sodium act as fluxing agents and result in the formation of lower melting phases. The solidus and liquidus temperatures of the silicate mixture therefore depend on the overall composition of the gangue, which range between 1100 and 1600 °C (Eksteen et al., 2011; Jones, 2005; Shaw et al., 2013).

Before the complete melting of the silicates with the subsequent generation of a liquid slag layer, the sintering of the concentrate bed takes place. This is a dynamic process as the temperature gradient and the thermal properties of the black top change from the freeboard towards the black top – slag interface. Matte drainage, changes in particle size distribution, changes in the phase chemistry of the minerals, as well as the generation and combustion of gases take place during sintering (Eksteen, 2011).

A schematic view of the different degrees of sintering expected in the black top as a function of temperature is shown in Figure 1. From the high degree of heterogeneity in the PGM concentrates (in terms of minerals and their relative amounts), it can be postulated that both solid state and liquid state sintering take place in the black top.

[Figure 1 near here]

Materials and methods

PGM concentrates

Two PGM concentrates were used in the experiments: UG–2 and Platreef. These concentrates were chosen because their exploitation is the current base of PGM processing in South Africa.

Experimental setup

The PGM concentrates were heated for two hours (heating rate of 10 °C min^{-1}), at eight different temperatures: 800, 900, 1000, 1100, 1200, 1300, 1400 and 1480 °C in a muffle furnace, purged with argon gas. Two hours of reaction time was chosen as this is the approximate time it takes the concentrate to move down the black top and into the slag layer. Silica (SiO_2) crucibles were used for the experiments with Platreef concentrate, while magnesia (MgO) crucibles were used when UG–2 concentrate was reacted. Although both concentrates are enriched in silica, the high MgO and FeO content of the UG-2 concentrate warranted the choice of magnesia crucibles for the UG-2 experiments. All the crucibles were filled with concentrate up to 5 mm below the rim (~ 17 grams of concenrate). The crucibles were gently tapped in order to level the surface of the concentrate, with the lowest degree of consolidation. The experiments were carried out in sealed steel capsules under argon atmosphere and cooled down inside the furnace (Figure 2) under argon. This configuration prevented the escape of sulphur–containing gases during the experiments.

[Figure 2 near here]

Characterization techniques

The chemical compositions of the bulk concentrates were determined using Inductively Coupled Plasma – Optical Emission Spectroscopy (ICP–OES) and a LECO Sulphur Analyser. The crystalline phases were identified with X–ray diffraction (XRD), using a PANalytical X'pert Pro powder diffractometer with Co Kα radiation (λ=1.789Å), employing the ICSD (Inorganic Crystal Structure Database) and X'Pert Highscore Plus software. The quantification of crystalline phases was obtained by Rietveld refinement of the XRD patterns.

The raw PGM concentrates as well as fired samples were prepared for metallographic analyses. Polished sections were prepared by using AKASEL epoxy resin which was cured at 70 °C for 24 hours. After curing, the samples were ground by using silicon carbide paper (from 200# to 1200#) and polished with diamond suspensions of 9.0, 6.0 and 1.0 μm.

The polished sections were coated in a Quantum carbon coater. A Jeol JSM–IT300LV scanning electron microscope (SEM) coupled with an Oxford X–Max 50 Energy–Dispersive X–ray Spectrometer (EDS) was used for microstructural as well as phase analyses. All the EDS spectrums were individually processed and refined after acquisition.

Thermochemical predictions

Observed phase relations were compared against phase relations predicted by FactSage® 7.3 (Bale et al., 2016). The liquid content in the PGM concentrates at different temperatures was obtained from the Equilib module, using the FactPS and FToxid databases. The sulphur partial pressure was obtained from the Predom module

(Fe–S–O system), for all the studied temperatures and their respective oxygen partial pressures.

The oxygen partial pressures used in the predictions were calculated from the iron–wüstite (Fe/FeO) oxygen buffer, while the sulphur partial pressure was calculated based on the iron–troilite (Fe/FeS) sulphur buffer. The oxygen partial pressures used in the calculations ranged from 10^{-18} bar (800 °C) to 10^{-9} bar (1480 °C); and the predicted sulphur partial pressures ranged from 10^{-9} bar (800 °C) to $10^{-3.5}$ bar (1480 °C).

Results

Chemical composition

The ICP–OES and XRF analyses of the UG–2 and Platreef concentrates are shown in Table 1. The most significant differences between the two concentrates are the higher amounts of silicon and magnesium oxides in the UG–2 concentrate, and the higher concentrations of base metals (nickel and copper) and sulphur in the Platreef concentrate. Another significant difference is the higher amount of chromium oxide in the UG–2 concentrate.

[Table 1 near here]

The concentrations of the different components and elements in the UG–2 and Platreef concentrates are shown in Figure 3. The maximum and minimum values for each component as reported in the literature are represented by the dashed lines. The major components of both concentrates agree well with the values found in the literature for UG–2 and Platreef PGM concentrates (Adams et al., 2011; Barnes & Newall, 2006; F. Crundwell, 2011; Eksteen et al., 2011; Jones & Kotzé, 2004; Muzawazi & Petersen, 2015; Mwase et al., 2012).

[Figure 3 near here]

Mineralogical composition

The quantification of the crystalline phases by Rietveld refinement is shown in Table 2. The mineral compounds found in both concentrates can be divided in two main groups: gangue components and sulphides.

Talc ($Mg_3(Si_2O_5)_2(OH)_2$) and enstatite ($(Mg,Fe)_2Si_2O_6$) constitute 75.18% of the UG–2 concentrate and 66.60% of the Platreef concentrate. The concentrates significantly differ in the sulphides content (1.32% for UG–2 and 17.33% for Platreef), while chromite ($(Fe^{2+},Mg)(Cr,Al,Fe^{3+})_2O_4$) was only found in the UG–2 concentrate (2.88%). The sulphide minerals pentlandite and chalcopyrite are present in both the UG-2 and Platreef concentrates, while the Platreef concentrate also contains measurable amounts of pyrite.

[Table 2 near here]

Prediction of melting behaviour by FactSage®

The expected liquid contents of both concentrates under equilibrium conditions (as predicted by FactSage®) at temperatures from 800 to 1480 °C is shown in Figure 4. From 800 to 1100 °C, the predicted amounts of liquid in UG–2 and Platreef concentrate are negligible. When the concentrates are heated at 1200 °C, the amount of liquid increases to 32.5% and 0.22% in the Platreef and UG–2 concentrates, respectively. This difference in the amounts of liquid present in the Platreef and UG–2 concentrates increases at 1300 °C and 1400 °C, while at 1480 °C both concentrates exhibit similar

amounts of liquid (99.9% for Platreef and 99.7% for UG–2).

[Figure 4 near here]

The solidus temperature of the gangue of the Platreef concentrate is predicted by FactSage to be 1100 °C, with pyroxene as primary phase, while the predicted solidus temperature of the gangue of he UG-2 concentrate is 1250°C with the chromium-containing spinel as primary phase.

Macroscopic inspection of fired samples

A marked increase in shrinkage occurred at temperatures above 1200 °C for the Platreef charge, while from above 1300 °C for the UG-2 charge (Figure 5). The shrinkage is consistent with the steep increase in the liquid content as predicted by FactSage® (Figure 4).

[Figure 5 near here]

The UG–2 concentrate exhibited a small degree of consolidation and sintering of the powder from 800 to 1300 °C. At 1400 °C this concentrate exhibited a highly porous but sintered structure; however, the separation of matte and slag was still not detectable. The formation of a matte button at the bottom of the crucible confirmed that matte–slag separation took place at 1480 °C (Figure 6), as shown in the area enclosed by the black rectangle in Figure 6 (b). The backscattered electron image (BEI) of the matte button–slag interface from Figure 6 (b) is presented in Figure 7. Accumulation of matte through the formation of a matte button was observed, although small matte droplets could still be observed in the slag.

[Figure 6 near here]

[Figure 7 near here]

Similar observations were made of the Platreef concentrate that was reacted from 800 to 1200 °C. However, at 1300 °C matte already accumulated in a button at the bottom of the crucible. Some of the matte also collected on the top surface of the fired concentrate (Figures 8 (a) and (b)).

[Figure 8 near here]

At 1400 °C (Figure 9) the Platreef concentrate exhibited porosity as well as shrinkage, with several matte droplets being attached to the pores. The effective separation of matte and slag in the concentrate was evidenced through the formation of a matte button at the bottom of the crucible (Figure 10). The top surface of the Platreef concentrate reacted at 1480 °C showed a glassy texture and separation of a matte button from the slag. This glassy texture was only observed in the Platreef concentrate and only at 1480 °C (Figures 11 (a) and (b)). It consisted of elongated matte zones dispersed in the glass, with no porosity (Figure 11 (c)).

[Figure 9 near here]

[Figure 10 near here]

[Figure 11 near here]

Mineralogical composition of fired samples

The major crystalline phases that are present in the gangue component of the UG–2 and

Platreef concentrates at different temperatures, as determined by quantitative XRD, are given in Figures 12 and 13. The concentration of enstatite in the UG–2 concentrate increases from 800 to 1300 °C. Enstatite and augite [$(Ca,Mg,Fe)_2(Si,Al)_2O_6$] are the major phases at 1480 °C. Platreef concentrate exhibited a similar trend, with the amount of enstatite increasing from 800 to 1300°C, but with a significant increase in anorthite ($CaAl_2Si_2O_8$) content at 1400°C and augite at 1480 °C.

It was verified that matte drainage occurs at sub–liquidus temperatures of the gangue component of the concentrate. In the UG–2 concentrate matte drainage occurred at 1480 °C, while in the Platreef concentrate it occurred at both 1400 and 1480 °C. In both the UG-2 and Platreef concentrates matte drainage was accompanied by a decrease in enstatite content in the concentrates.

[Figure 12 near here]

[Figure 13 near here]

Microstructural analysis

The BEIs of the UG–2 concentrate fired at 800, 900, 1000 and 1100 °C are shown in Figure 14. At all of these temperatures there is evidence of reactions within particles (indicated as RS, reacted silicate) with an accompanied increase in porosity of the silicate phase. This presumably reflects the dehydroxylation of certain of the silicate minerals. However, there is no evidence of the formation of a liquid phase (LP) or noticeable sintering.

[Figure 14 near here]

The BEIs of the UG–2 concentrate fired at 1200, 1300, 1400 and 1480 °C are shown in Figure 15. A liquid phase can be distinguished in all of these BEIs. At 1200 °C, the previously loose particles have developed a sintered microstructure with silicate particles interconnected by necks, as typically observed at early stages of the sintering process (Figure 15). Some matte droplets remained entrained within the cavities generated in the sintering process, while the precipitation of the chromium-rich spinel from the matte particles could be verified. Enstatite is the most abundant phase, with some of the crystals partially surrounded by the LP, which acted as bonding phase. The melt is constituted by SiO_2 (61.5%), Al_2O_3 (19.5%), CaO (6.7%), MgO (5.1%), FeO (2.3%) and Na_2O (2.2%); with minor amounts of K_2O (0.8%), Cr_2O_3 (1.5%) and TiO_2 (0.5%).

[Figure 15 near here]

At 1300 °C there was a coarsening of the bonds between particles, while the particles themselves increased in size (Figure 15). A higher amount of LP, surrounding the enstatite crystals, is present at 1300 °C than at 1200 °C. The chemical composition of the LP exhibits a decrease in SiO_2 and MgO, which is consistent with the increase in the amount of enstatite detected by XRD. The increase in FeO content of the LP from 2.3 to 6.1% is also consistent with the decreased FeO content in the enstatite.

The reaction between the LP and enstatite resulted in a cored microstructure (Figure 16). This is an indication that equilibrium was not maintained when the samples were cooled in the furnace. The precipitation of the Fe-rich solid solution phase occurred mainly as a thin rim (1.0 – 3.0 μm in width), which could not accurately be analysed by SEM–EDS because of the size of the interaction volume (~10 μm diameter) that exceeds the thickness of the rim. However, point analysis suggests an enrichment in CaO and Al_2O_3 together with a decrease in MgO content in the rim. The centre of these

enstatite crystals (En(cored), Figure 16) are enriched in iron. Un–cored particles could also be distinguished (En (uncored), Figure 16). These crystals contain lower concentrations of iron and higher concentrations of magnesium.

[Figure 16 near here]

UG–2 concentrate still exhibited some remaining porosity after firing at 1400 °C, while Platreef concentrate displayed a dense microstructure. At 1400 °C, the LP became a continuous phase that surrounded the remaining crystals in the system. The decrease of MgO in the LP suggests the crystallisation of enstatite and augite from the LP, with a subsequent increase in FeO content of the LP. Augite crystals resulted from two sources at this temperature: the reaction between enstatite and the liquid phase to form augite and the dendritic precipitation of augite crystals from the bulk LP on cooling. The chemical compositions of the augite crystals that formed are $(Ca_{0.55}Fe^{2+}_{0.46}Na_{0.01}K_{0.01})_{\Sigma=1.03}(Mg_{0.57}Al_{0.26}Ti_{0.03}Cr_{0.01})_{\Sigma=0.87}(Si_{1.90}Al_{0.10})_{\Sigma=2}O_6$ and $(Ca_{0.44}Fe^{2+}_{0.13}Na_{0.05})_{\Sigma=0.62}(Mg_{0.97}Al_{0.28}Cr_{0.01}Ti_{0.01})_{\Sigma=1.27}(Si_{1.99}Al_{0.01})_{\Sigma=2}O_6$ in the UG–2 and Platreef concentrates, respectively. The dendritically precipitated augite crystals are however too small for accurate EDS analysis (< 5 μm in diameter).

At 1480 °C, the amount of LP has dramatically increased, as can be seen from Figures 6 (b) and 15 where the porosity in the concentrate has virtually disappeared. The enstatite crystals do not exhibit the coring effect observed at 1300 and 1400 °C, but have started to show a columnar habit, due to sintering.

The BEIs of the Platreef concentrate fired at 800, 900, 1000 and 1100 °C are shown in Figure 17. The behaviour of the gangue minerals is similar to that observed in

the UG–2 concentrate, i.e. dehydroxylation reactions of gangue minerals (RS) took place, but no sintering or LP formation was observed.

[Figure 17 near here]

The microstructures of Platreef concentrate fired at 1200, 1300, 1400 and 1480 °C are shown in Figure 18. A liquid phase can be distinguished in all of these samples. At 1200 °C enstatite is the dominant phase as confirmed by XRD. The enstatite exhibits the same coring effect observed in the UG–2 concentrate at 1300, 1400 and 1480 °C.

[Figure 18 near here]

After firing at 1300 °C, the LP is already a continuous phase which surrounds the existing crystals. The MgO content of the LP decreases from 4.1 to 2.2% and the FeO increases from 1.6 to 3.7%, this compositional change is consistent with the consumption of MgO in enstatite during crystallisation. It was also possible to distinguish some sintered enstatite aggregates in which a LP was observed. Augite formed on the boundaries of the enstatite crystals, but some augite crystals also separated from the enstatite crystals and could be found in the liquid phase. No dendritic augite crystals were observed in this concentrate at this temperature.

At 1400 °C, the largest variations in the chemical composition of the LP are the increase in SiO_2 content from 63.8 to 65.4% because of the decomposition of enstatite and the decrease in Al_2O_3 from 20.0 to 17.9%. The decrease in Al_2O_3 can be attributed to the consumption of this component through the formation of Al_2O_3–containing phases, such as anorthite and augite, as shown by XRD. The enstatite crystals started

merging with each other and formed longer aggregates. At this temperature there is virtually no chemical gradient within the enstatite crystals. Only the thin rim at the enstatite–melt interface is noticeably different. The sudden increase in augite content at this temperature was confirmed by the precipitation of dendritic augite crystals from the LP on cooling. The augite crystals that formed on the enstatite boundaries have also increased in size. The columnar habit of the enstatite crystals is shown in Figure 19.

[Figure 19 near here]

The concentrate seemed to be completely molten at 1480 °C. The columnar growth of enstatite (dark grey crystals) with different crystal orientations is noticeable in the top surface of the concentrate after it was cooled from 1480ºC in the furnace (Figure 20). These columnar enstatite crystals with different crystal orientations are also visible in the bottom part of the crucible. Some of the matte has been squeezed on cooling from the bottom of the crucible to upper positions in the concentrate, occupying some of the space between the columnar enstatite crystals (Figure 21).

[Figure 20 near here]

[Figure 21 near here]

Discussion

Although the decomposition of gangue minerals in both UG–2 and Platreef concentrates starts to take place from 800 °C, the sintering of the gangue minerals only begins at firing temperatures of 1200 °C. Both concentrates exhibited increased densification of their microstructures and a decrease in porosity with increasing temperature, along with

the merging of enstatite crystals to form larger columnar crystals. These observations suggest that liquid phase sintering dominates sintering in both PGM concentrates (German et al., 2009).

The formation of a liquid phase in both concentrates at temperatures of 1200 °C and higher was evidenced by the shrinkage and sintering of the concentrates. This onset of liquid formation agrees with the FactSage® predicted solidus temperatures of above 1100 °C and above 1200 °C for respectively the Platreef and UG-2 concentrates. The liquidus temperature predicted by FactSage® for the Platreef concentrate is consistent with what was observed experimentally. However, as the FactSage® predicted liquidus temperature of 1600 °C for the UG–2 concentrate substantially exceeds the maximum operational temperature of the steel capsules (~ 1515 °C, Gorni, 2003) it was not possible to confirm this value with the current experimental setup. However, this predicted liquidus temperature for the UG–2 concentrate is consistent with other studies which reported liquidus temperatures in the order of 1600 °C, and typical slag operational temperatures of 1460 - 1650 °C for high chromium-containing PGM concentrates (Nell, 2004; Shaw et al., 2013; Somerville et al., 2004).

The separation of matte and slag, and the accumulation of a matte button at the bottom of the crucible, was successful after firing the UG–2 concentrate at 1480 °C. The high degree of shrinkage of the concentrate bed at this temperature is accompanied by a sudden decrease in enstatite content and the formation of augite and an olivine phase (Mg_2SiO_4). This suggests that a liquid phase is generated when enstatite (the main gangue component) decomposes. According to the literature the decomposition of pure enstatite takes place at 1556 °C through a peritectic reaction during which forsterite (Mg_2SiO_4) is formed (Frost and Frost, 2014). However, the temperature at which liquid formation starts when a $Mg_2Si_2O_6$ – $Fe_2Si_2O_6$ solid solution phase decomposes, is

decreased with increasing $Fe_2Si_2O_6$ content of the solid solution phase (Ohi and Miyake, 2016). The average $Fe_2Si_2O_6$ content of the enstatite phase in the UG-2 and Platreef concentrates, as determined by EDS, was found to be 6.2 ± 2.31 mass% and 9.9 ± 3.30 mass% respectively. The enstatite present in the Platreef concentrate therefore decomposes at lower temperatures than the enstatite in the UG-2 concentrate.

The Platreef concentrate exhibited successful matte separation after firing at both 1400 °C and 1480 °C. The high amount of liquid predicted by FactSage® at these temperatures is reflected in the concentrate bed shrinkage. The microstructural analysis also showed a continuous and dominant LP which acts, similar to the UG–2 concentrate, as a path that promotes matte drainage and its accumulation as a button at the bottom of the crucible. At 1300 °C the amount of liquid in the Platreef concentrate was already enough to allow matte droplets to descend through the continuous LP whereby matte–slag separation became feasible, although not complete. FactSage calculations predicted that 51.7% liquid was present at this temperature.

The main decomposition reactions of the sulphides that are commonly found in PGM concentrates are given in Table 3 (Eksteen, 2011). It is evident that the matte is already fully molten when the PGM concentrates start to sinter at 1200 °C. The Platreef concentrate still exhibited a high degree of porosity and sintering after firing at 1300 °C, but it still remained as a sintered bulk structure as shown in Figures 8 (a) and (b).

[Table 3 near here]

The conditions under which slag–matte separation was effective is summarised in Table 4. Separation and collection of matte in a button was only feasible after a high amount of liquid has formed (52% in the Platreef concentrate and 99% in the UG-2 concentrate). The high amount of liquid provides a continuous liquid path through which the matte can descend (because of its higher density) and finally accumulate at

the bottom of the crucible as a matte button. It can however be assumed that the viscosity of this liquid phase will impact on matte accumulation.

[Table 4 near here]

Despite exhibiting a continuous LP, the UG–2 concentrate fired at 1400 °C did not exhibit successful matte separation, probably because the enstatite did not completely melt. The amount of liquid in the UG-2 concentrate bed was therefore not enough to allow matte droplets to settle and collect. Guntoro et al. (2018) studied matte – slag separation in a concentrate consisting of fayalite and chalcopyrite at 1300 °C in air and argon. They observed that matte coagulation only occurs after a substantial amount of liquid slag was formed, both in air and in argon. Similar observations about the necessary conditions for matte settling after coalescence were reported by Fagerlund and Jalkanen (2001) for a copper sulphide matte settling through a liquid wollastonite slag. It is important to highlight that in the present study, the lower amount of sulphides in the UG–2 concentrate compared to the Platreef concentrate, entails a much higher degree of dispersion of smaller molten sulphide (matte) droplets. This condition represents a hindrance for these matte droplets to coalesce, increase in size, and settle through the pathways of molten slag that formed within the sintered bed.

Conclusions

UG–2 concentrate contains significantly higher amounts of silicon, magnesium and chromium oxides than Platreef concentrate. Talc and enstatite constitute 75.18% of the UG-2 concentrate and 66.60% of the Platreef concentrate, while chromite is only found in the UG-2 concentrate. Platreef concentrate however contains significantly higher concentrations of iron, nickel and copper sulphides (17.3 vs. 1.3%).

Talc decomposes mainly to enstatite at temperatures from 800 °C in both the UG–2 and Platreef concentrates. Enstatite in these concentrates is a $Mg_2Si_2O_6$ – $Fe_2Si_2O_6$ solid solution phase. The $Fe_2Si_2O_6$ content of this solid solution phase is higher in the Platreef concentrate than in the UG-2 concentrate, which implies that the enstatite starts to decompose incongruently into a liquid phase at lower temperatures. The FactSage predicted solidus temperatures of above 1100 °C for the Platreef concentrate and 1200 °C for UG-2 concentrate agree well with the experimental results.

The commencement of liquid phase formation causes shrinkage of the black top due to liquid phase sintering. The amount of liquid that forms in the Platreef concentrate is higher than in the UG–2 concentrate due to its lower liquidus temperature. The liquidus temperature of the PGM matte is below the solidus temperatures of the concentrates, which implies that the matte is fully molten when sintering starts.

Matte drainage and collection through the concentrate bed occur at temperatures below the liquidus temperatures of the gangue minerals, but above their solidus temperatures.

Acknowledgments

The authors gratefully thank Anglo American for their financial and technical support. Ms Wiebke Grote and Prof. Johan de Villiers are acknowledged for their help with the

XRD analysis, while Dirk Odendaal is thanked for his assistance in the laboratory.

Declaration of interest statement

The authors have no conflict of interest to declare.

References

Adams, M., Liddell, K., and Holohan, T. (2011). "Hydrometallurgical processing of Platreef flotation concentrate." *Minerals Engineering*, *24*(6), pp. 545–550.

Bale, C. W., Bélisle, E., Chartrand, P., Decterov, S. A., Eriksson, G., Gheribi, A. E., Hack, K., Jung, I. H., Kang, Y. B., Melançon, J., Pelton, A. D., Petersen, S., Robelin, C., Sangster, J., Spencer, P., and Van Ende, M. A. (2016). "FactSage thermochemical software and databases, 2010-2016." *Calphad: Computer Coupling of Phase Diagrams and Thermochemistry*, *54*, pp. 35–53.

Barnes, A. R., and Newall, A. F. (2006). "Spinel removal from PGM smelting furnaces." *Southern African Pyrometallurgy*, *March*, 5–8.

Belgacem, K., Llewellyn, P., Nahdi, K., and Trabelsi-Ayadi, M. (2008). "Thermal behaviour study of the talc." *Optoelectronics and Advanced Materials, Rapid Communications*, *2*(6), pp. 332–336.

Crundwell, F. (2011). *Extractive Metallurgy of Nickel and Cobalt* (F. K. Crundwell, M. S. Moats, V. Ramachandran, T. G. Robinson, & W. G. Davenport (eds.)). Elsevier Ltd. https://www.sciencedirect.com/book/9780080968094/extractive-metallurgy-of-nickel-cobalt-and-platinum-group-metals

Eksteen, J. J. (2011). "A mechanistic model to predict matte temperatures during the smelting of UG2-rich blends of platinum group metal concentrates." *Minerals Engineering*, *24*(7), pp. 676–687.

Eksteen, J. J., Van Beek, B., and Bezuidenhout, G. A. (2011). "Cracking a hard nut: An overview of Lonmin's operations directed at smelting of UG2-rich concentrate blends." *Journal of the Southern African Institute of Mining and Metallurgy*,

111(10), pp. 681–690.

Ewell, B. R. H., Bunting, E. N., and Geller, R. F. (1935). "Thermal decomposition of talc." *National Bureau of Standards*, *15*.

Fagerlund, K. O., and Jalkanen, H. (2001). "Microscale Simulation of Settler Processes in Copper Matte Smelting." *Metallurgical and Materials Transactions B: Process Metallurgy and Materials Processing Science*, *32*(3), 555–557.

Frost, B. R., and Frost, C. D. (2014). *Essentials of Igneous and Metamorphic Petrology* (C. U. Press (ed.); First).

German, R. M., Suri, P., and Park, S. J. (2009). "Review: Liquid phase sintering." *Journal of Materials Science*, *44*(1), pp. 1–39.

Gorni, A. A. (2003). *Steel Forming and Heat Treating Handbook* (Issue 13 December 2019).

Guntoro, P. I., Jokilaakso, A., Hellstén, N., and Taskinen, P. (2018). "Copper matte - slag reaction sequences and separation processes in matte smelting." *Journal of Mining and Metallurgy, Section B: Metallurgy*, *54*(3), pp. 301–311.

Jones, R. T. (2005). "An overview of South African PGM smelting." *Nickel and Cobalt 2005: Challenges in Extraction and Production*, *January*, pp. 147–178.

Jones, R. T., and Kotzé, I. J. (2004). "DC arc smelting of difficult PGM-containing feed materials Feed materials." *International Platinum Conference 'Platinum Adding Value,'* pp. 33–36.

Muzawazi, C., and Petersen, J. (2015). "Heap and tank leaching of copper and nickel from a Platreef flotation concentrate using ammoniacal solutions." *Canadian Metallurgical Quarterly*, *54*(3), pp. 297–304.

Mwase, J. M., Petersen, J., and Eksteen, J. J. (2012). "Assessing a two-stage heap leaching process for Platreef flotation concentrate." *Hydrometallurgy*, *129–130*, pp. 74–81.

Nell, J. (2004). "Melting of platinum group metal concentrates in South Africa."

Journal of the South African Institute of Mining and Metallurgy, *104*(7), pp. 423–428.

Ohi, S. and Miyake, A (2016). "Phase transitions between high- and low-temperature orthopyroxene in the $Mg_2Si_2O_6$- $Fe_2Si_2O_6$ system." *American Mineralogist, 101, pp. 1414-1422.*

Schouwstra, R. P., Kinloch, E. D., and Lee, C. A. (2000). "A Short Geological Review of the Bushveld Complex | Johnson Matthey Technology Review." *Platinum Metals Review*, 44(1), pp. 33–39.

Shaw, A., De Villiers, L. P. V. S., Hundermark, R. J., Ndlovu, J., Nelson, L. R., Pieterse, B., Sullivan, R., Voermann, N., Walker, C., Stober, F., and McKenzie, A. D. (2013). "Challenges and solutions in PGM furnace operation: High matte temperature and copper cooler corrosion." *Journal of the Southern African Institute of Mining and Metallurgy*, *113*(3), pp. 251–261.

Singerling, S. A. (2019). "Platinum-Group Metals Statistics and Information." In *U.S. Geological Survey, Mineral Commodities Summaries*.

Sinisalo, P., and Lundström, M. (2018). "Refining Approaches in the Platinum Group Metal Processing Value Chain—A Review." *Metals*, *8*(4), p. 203.

Somerville, M., Wright, S., Sun, S., and Jahanshahi, S. (2004). "Liquidus temperature and viscosity of melter slags." *VII International Conference on Molten Slags Fluxes and Salts*, pp. 219–224.

Sahu, P., Jena, M. S., Mandre, N. R., and Venugopal, R. (2020). "Platinum Group Elements Mineralogy, Beneficiation, and Extraction Practices–An Overview." *Mineral Processing and Extractive Metallurgy Review*, pp. 1-14. DOI: 10.1080/08827508.2020.1795848

Table 1. Chemical compositions of the UG–2 and Platreef concentrates (mass %)

Concentrate	SiO_2	MgO	Fe	Ni	Al_2O_3	S	CaO	Cu	Cr	Na_2O	K_2O
UG–2	51.50	24.70	8.29	0.90	2.91	1.82	2.23	0.20	1.07	0.08	0.13
Platreef	41.40	15.80	14.80	4.09	3.57	12.80	2.86	2.12	0.12	0.48	0.11

Table 2. Quantitative XRD analysis of the UG–2 and Platreef concentrates.

Gangue compounds

UG–2 concentrate			Platreef concentrate		
Name	**Formula**	**wt. %**	**Name**	**Formula**	**wt. %**
Talc	$Mg_3 (Si_2 O_5)_2 (OH)_2$	39.70	Talc	$Mg_3 (Si_2 O_5)_2 (OH)_2$	39.27
Enstatite	$Fe_{0.438} Mg_{1.562} Si_2 O_6$	35.48	Enstatite	$Fe_{0.438} Mg_{1.562} Si_2 O_6$	27.33
Anorthite	$Al_{1.63} Ca_{0.64} Na_{0.35} Si_{2.37} O_8$	10.43	Augite	$Al_{0.17} Ca_{0.88} Fe_{0.28} Mg_{0.74} Mn_{0.01} Na_{0.03} Si_{1.87} Ti_{0.01} O_6$	5.88
Hornblende	$H_1 Al_{1.1} Ca_{1.7} Fe_{1.72} Mg_{3.44} Na_{0.46} Si_{6.9} O_{24}$	3.39	Clinochlore	$H_{16} Al_{2.884} Fe_{0.874} Mg_{11.126} Si_{5.116} O_{36}$	5.24
Clinochlore	$Mg_{4.54} Al_{0.97} Fe_{0.46} Mn_{0.03} (Si_{2.85} Al_{1.15} O_{10}) (OH)_8$	3.08	Actinolite	$(Mg, Ca, Fe, Na, Al, Mn, Ti)_7 (Na, K)_{0.16} (SiAl)_8 (OH)_{1.4} F_{0.46} O_{22}$	4.02
Chromite	$Al_{0.54} Cr_{1.46} Fe_{0.51} Mg_{0.49} O_4$	2.88	Lizardite	$H_4 Mg_3 (Si_2 O_5)_2 (OH)_2$	0.93
Olivine	Fe_2SiO_4	1.95			
Biotite	$K_{7.8} Na_{0.22} Mg_{1.63} Fe_{0.85} Ti_{0.33} Al_{1.35} Si_{2.84} (OH) O_{11}$	1.76			

Sulphide compounds

UG–2 concentrate			Platreef concentrate		
Mineral	**Formula**	**wt. %**	**Mineral**	**Formula**	**wt. %**
Pentlandite	$Fe_{17.68} Ni_{18.32} S_{32}$	0.89	Pentlandite	$Fe_{4.2} Ni_{4.8} S_8$	7.56
Chalcopyrite	$CuFeS_2$	0.43	Chalcopyrite	$CuFeS_2$	6.67
			Pyrite	$Fe_4 S_8$	3.10

Table 3. Decomposition reactions of the sulphides present in the PGM concentrates (Eksteen, 2011)

Reaction	Temperature (°C)
$Ni_9Fe_8S_{15} \rightarrow 3Ni_3S_2(s) + 8FeS(s) + 0.5S_2(g)$	650
$2CuFeS_2 \rightarrow Cu_2S(s) + 2FeS(s) + 0.5S_2(g)$	700
$Ni_3S_2(s) \rightarrow Ni_3S_2(l)$	789
$FeS_2 \rightarrow FeS(s) + 0.5S_2(g)$	796
$Cu_2S(s) \rightarrow Cu_2S(l)$	1129
$FeS \rightarrow FeS(l)$	1192

Table 4. Summary of slag–matte separation in both PGM concentrates at all studied temperatures

	Liquid content (%) (FactSage prediction)		State of concentrate bed		Slag–matte separation	
Temperature (°C)	UG–2	Platreef	UG–2	Platreef	UG–2	Platreef
800	0.16	0.83	Powder	Powder	No	No
900	0.18	0.96	Powder	Powder	No	No
1000	0.19	0.98	Powder	Powder	No	No
1100	0.20	2.00	Powder	Powder	No	No
1200	0.22	32.46	Sintered	Sintered	No	No
1300	26.23	51.65	Sintered	Sintered	No	Partially separated
1400	75.13	88.69	Sintered	Sintered	No	Successful
1480	99.73	99.92	Nearly molten	Molten	Successful	Successful

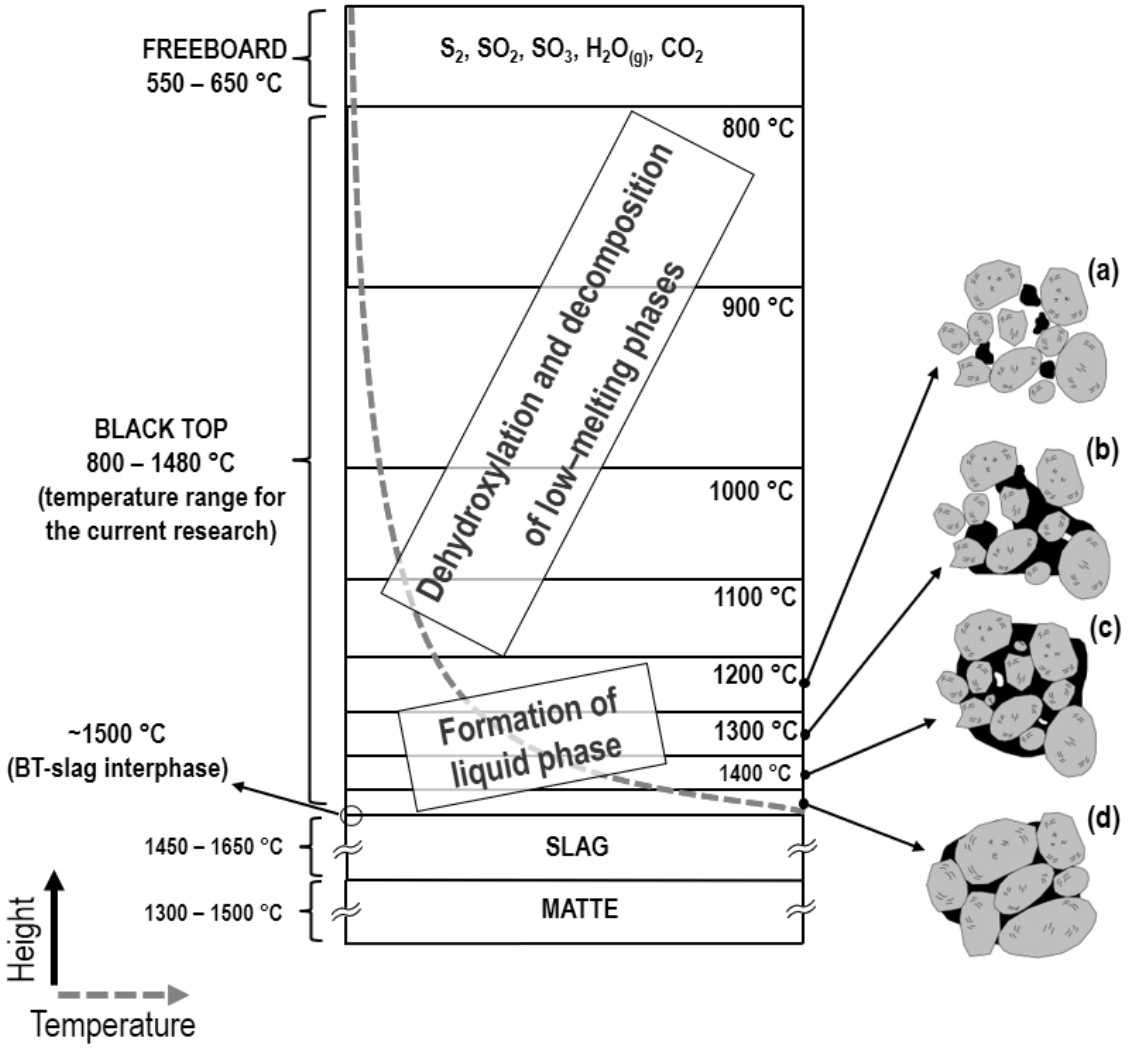

Figure 1. Schematic view of the black top with expected microstructures at (a) 1200 °C (b) 1300 °C (c) 1400 °C and (d) 1480 °C (the red line represents the temperature gradient). The black coloured phase in (a) to (d) represents a liquid phase.

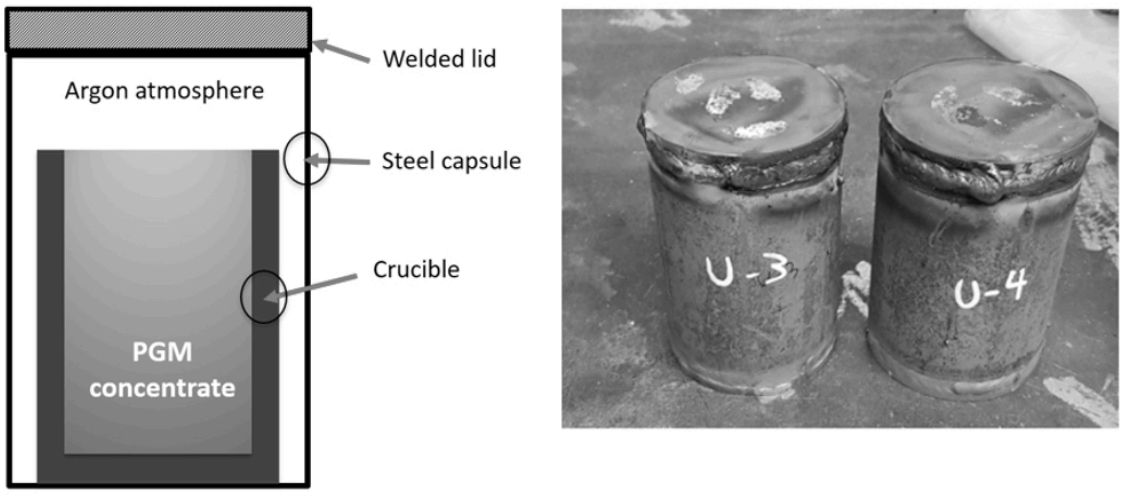

Figure 2. Schematic view of the sealed capsule system (left) and capsules after welding (right)

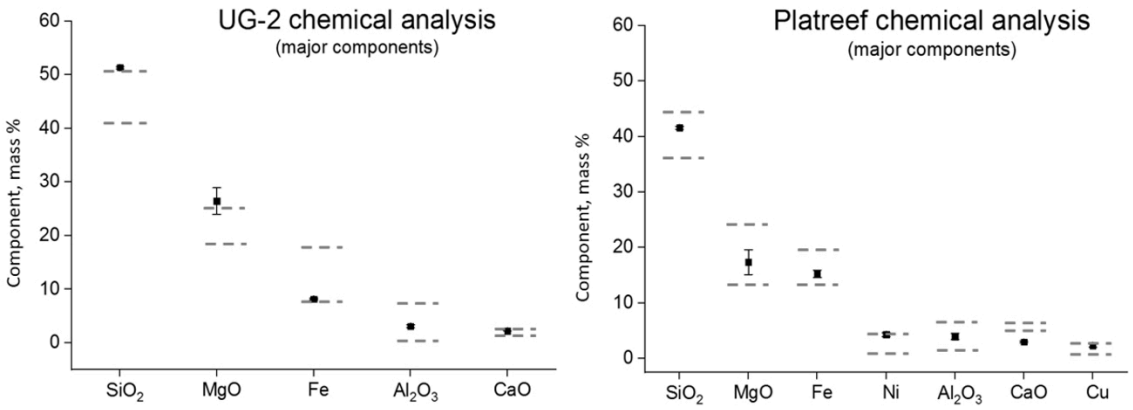

Figure 3. Chemical compositions of the PGM concentrates (black squares) and maximum and minimum values found in the literature (dashed lines)

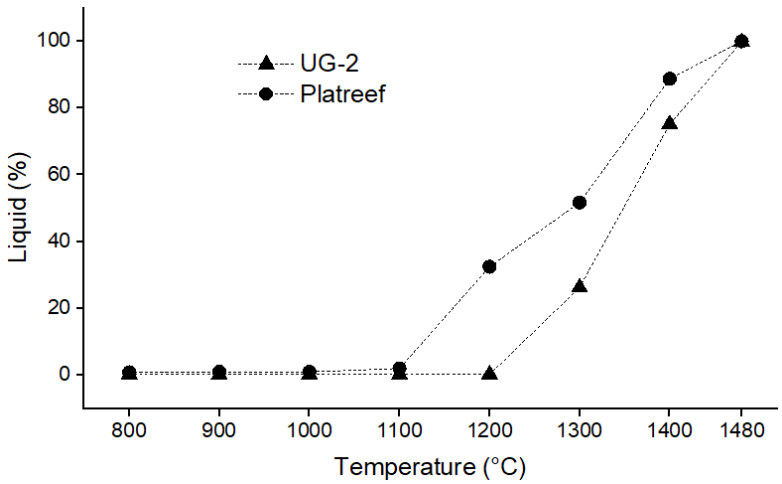

Figure 4. Liquid content in the concentrates as a function of temperature (predicted by FactSage®)

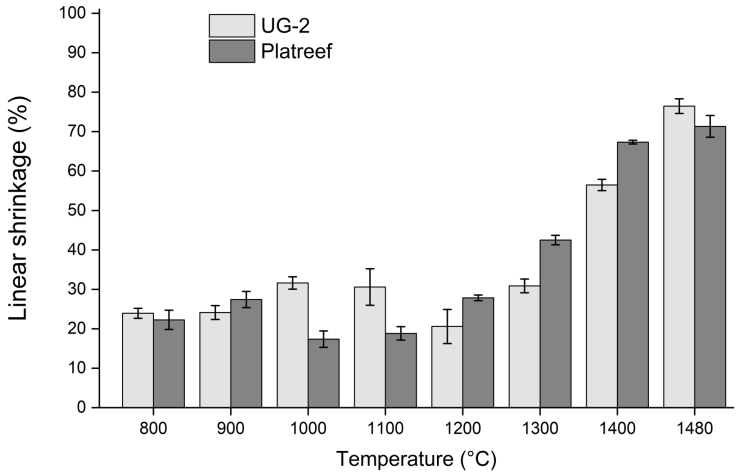

Figure 5. Linear shrinkage of the PGM concentrate samples after firing

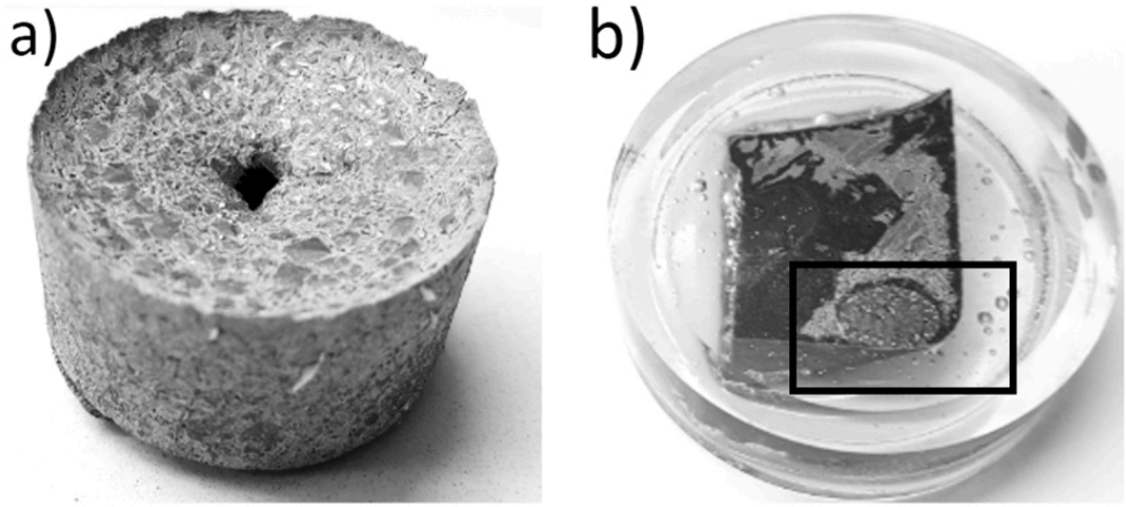

Figure 6. UG–2 concentrate fired at 1480 °C: (a) bulk fired concentrate;
(b) polished section showing a matte button at the bottom of the crucible

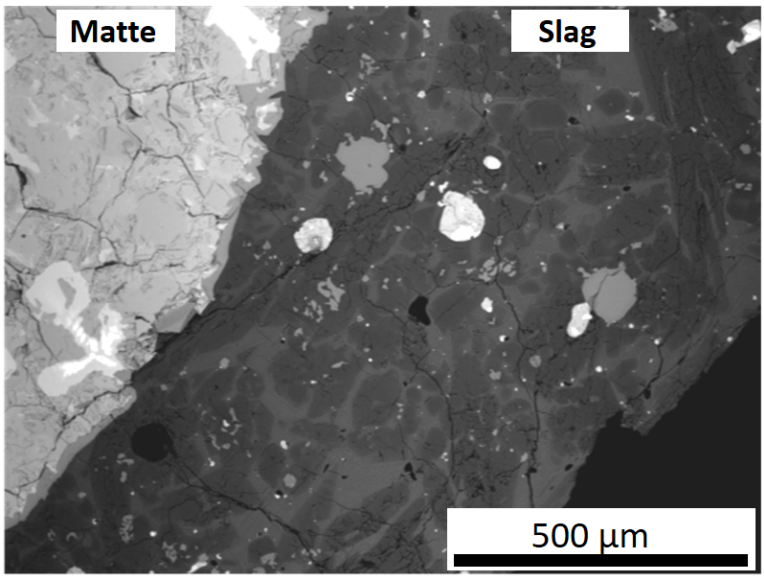

Figure 7. BEI of the UG–2 concentrate fired at 1480 °C showing the matte button–slag interfase

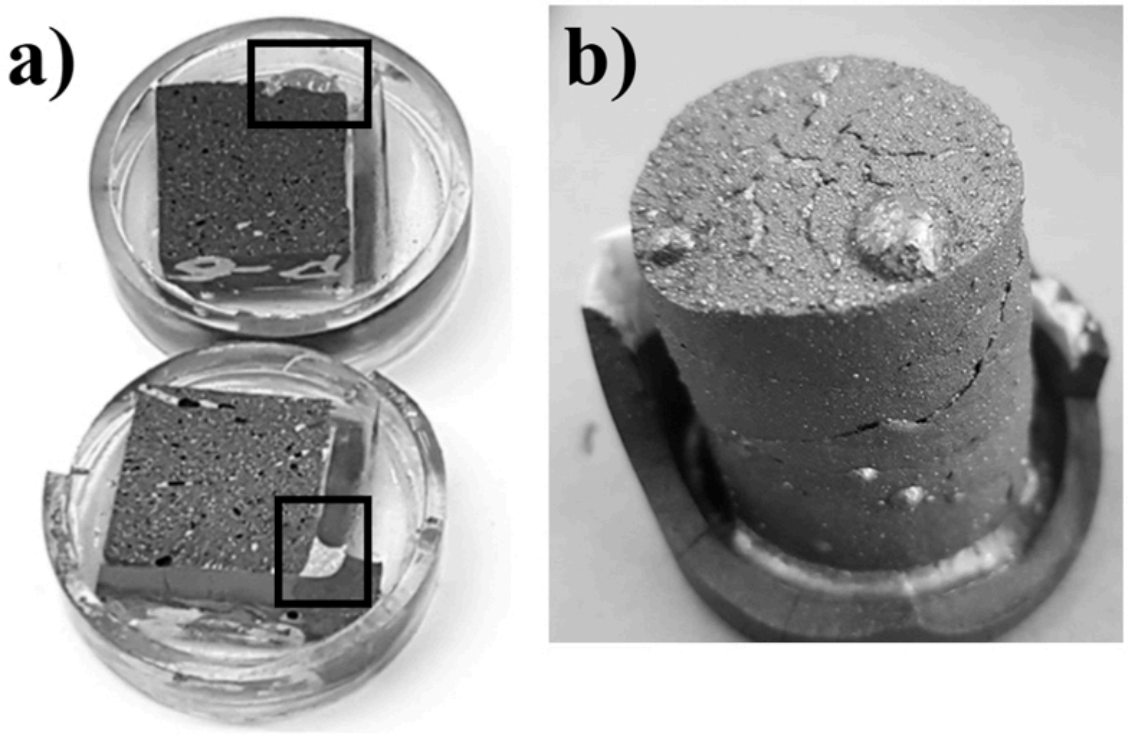

Figure 8. Platreef concentrate fired at 1300 °C: (a) polished sections (OD = 50 mm) of the top and bottom sections; (b) bulk fired concentrate

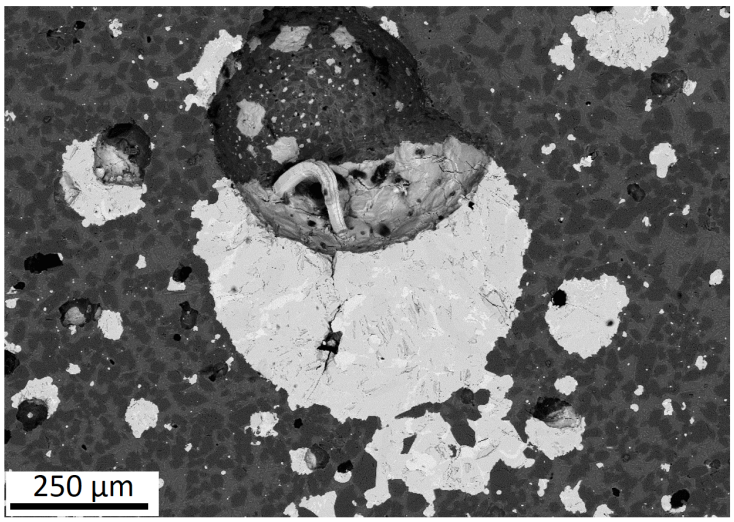

Figure 9. BEI of Platreef concentrate fired at 1400 °C

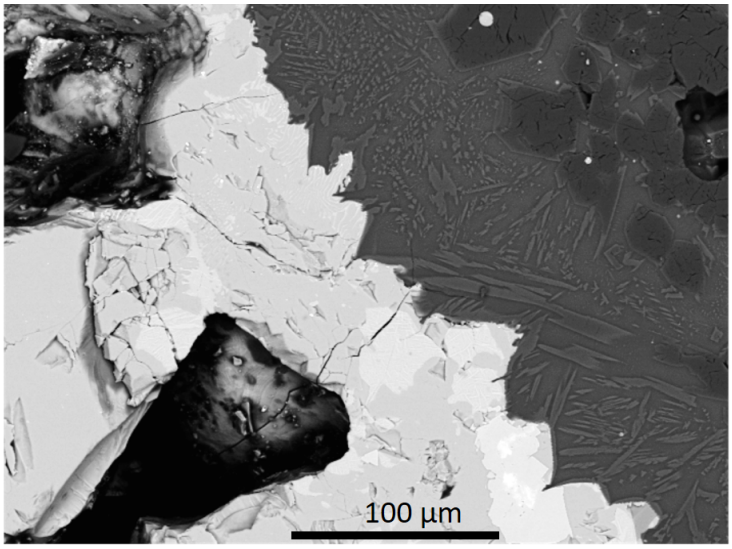

Figure 10. BEI of Platreef concentrate fired at 1400 °C

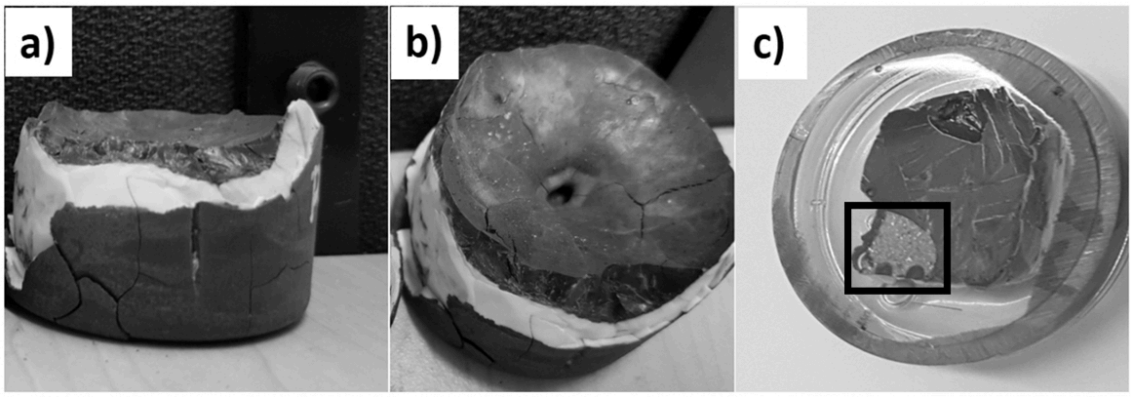

Figure 11. Platreef concentrate reacted at 1480 °C showing (a) side view, (b) top view and (c) polished section (OD = 50 mm)

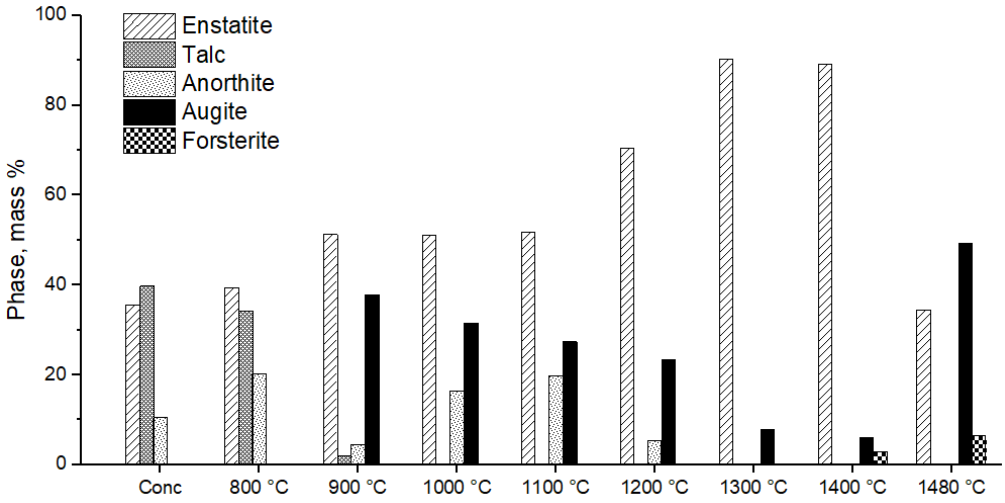

Figure 12. Major crystalline phases (UG–2 gangue) obtained after firing

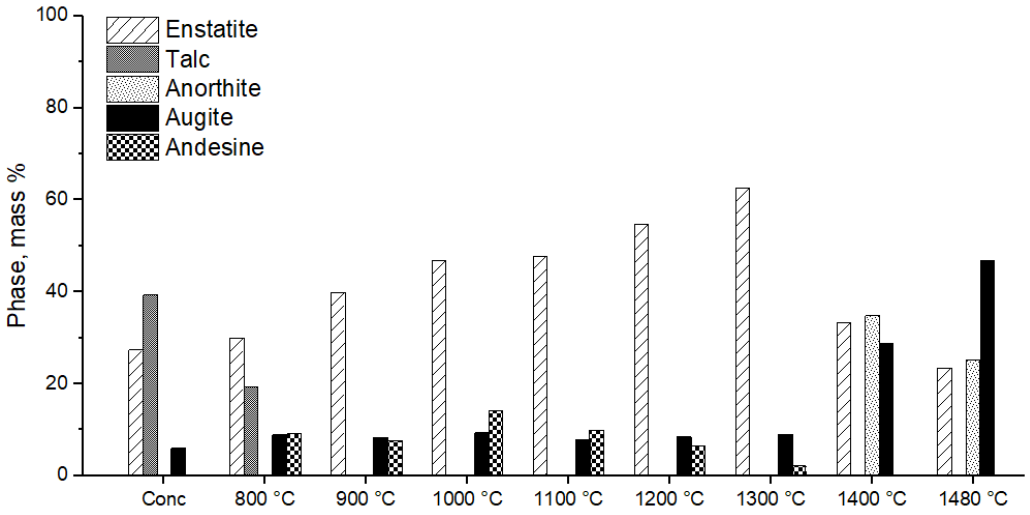

Figure 13. Major crystalline phases (Platreef gangue) obtained after firing

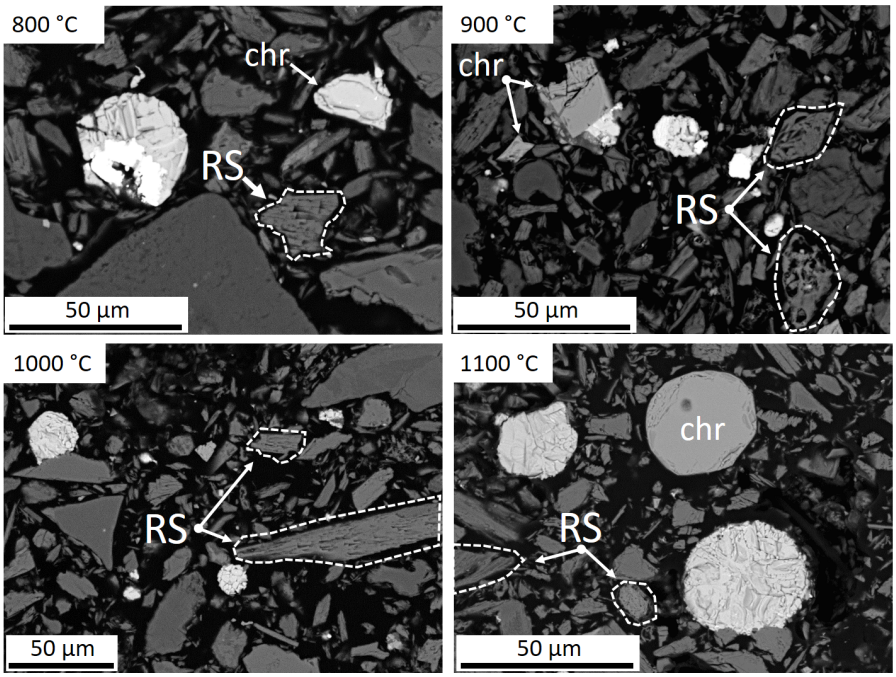

Figure 14. UG–2 concentrate fired from 800 to 1100 °C

(RS: reacted silicate; chr: chromite).

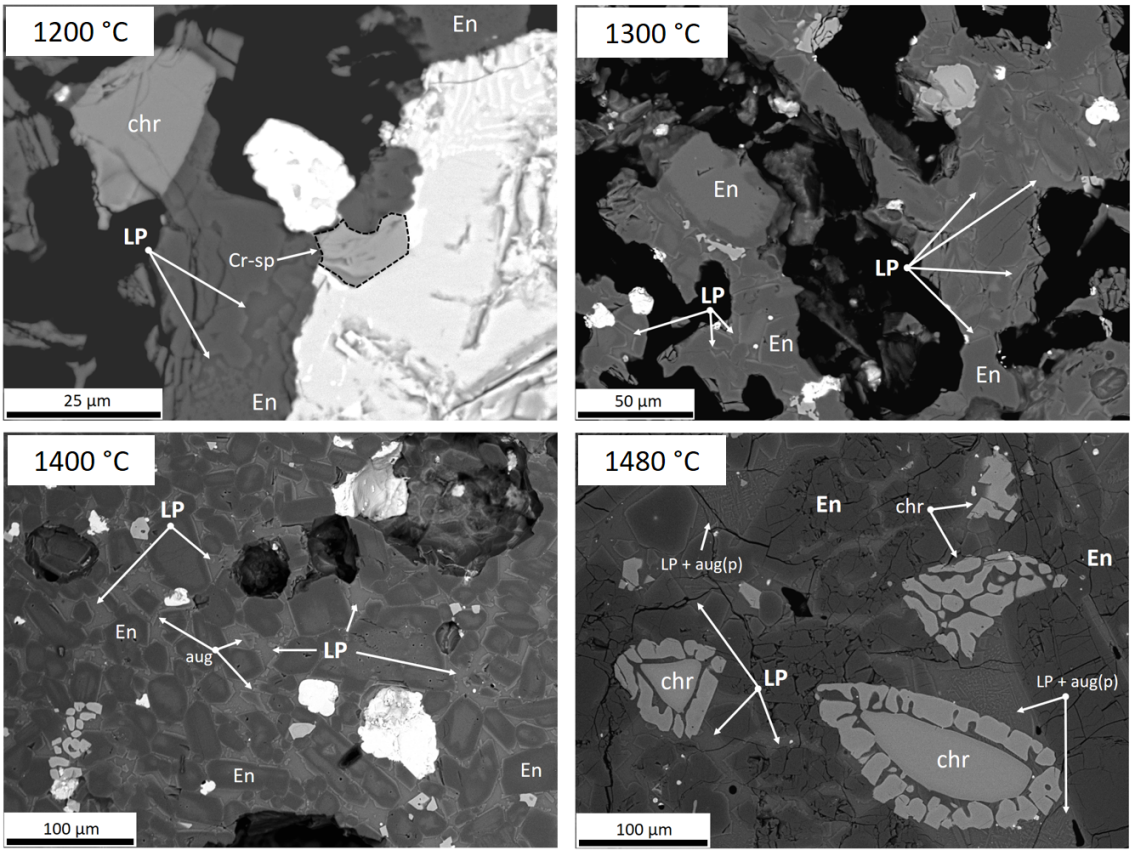

Figure 15. UG–2 concentrate fired from 1200 to 1480 °C (LP: liquid phase; En: enstatite; aug: augite; chr: chromite; Cr–sp: chromium-rich spinel).

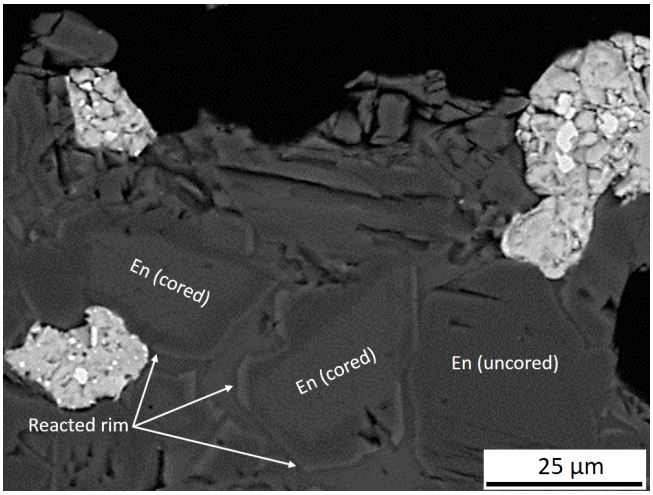

Figure 16. UG–2 concentrate fired at 1300 °C (En: enstatite).

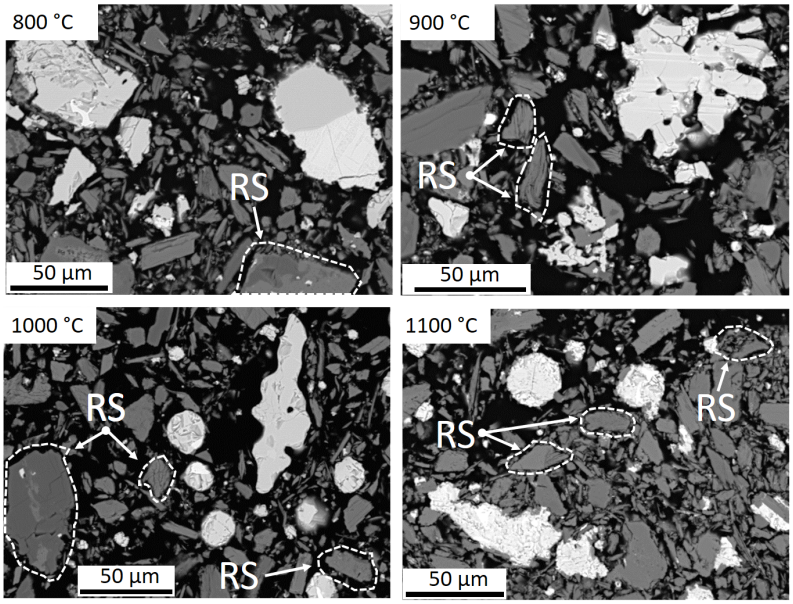

Figure 17. Platreef concentrate fired from 800 to 1100 °C (RS: reacted silicate).

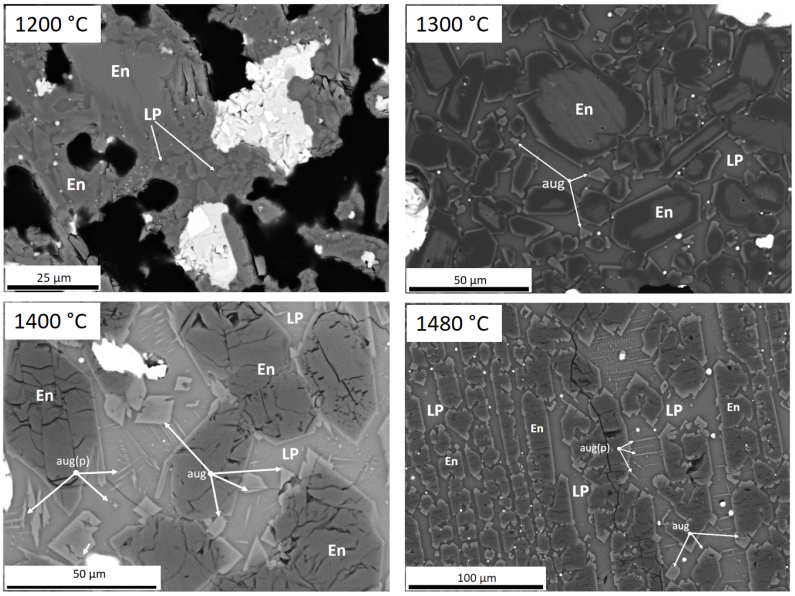

Figure 18. Platreef concentrate fired from 1200 to 1480 °C (LP: liquid phase; En: enstatite; aug: augite).

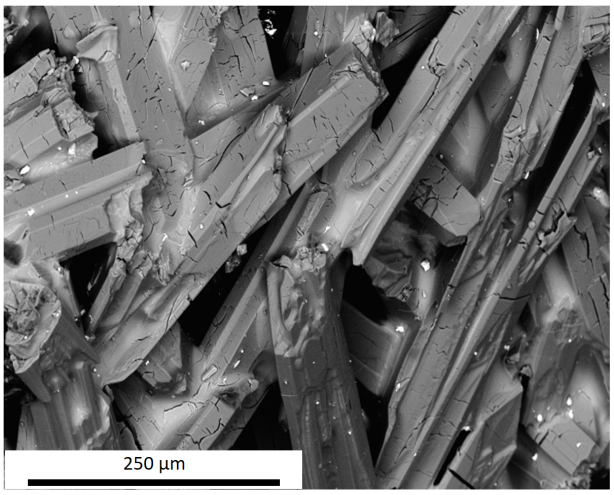

Figure 19. Columnar enstatite crystals in Platreef concentrate fired at 1400 °C (unpolished surface).

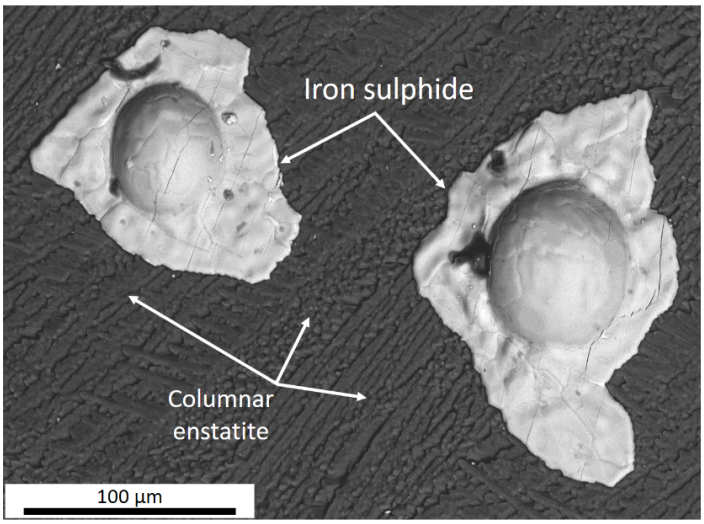

Figure 20. Platreef concentrate fired at 1480 °C (unpolished surface).

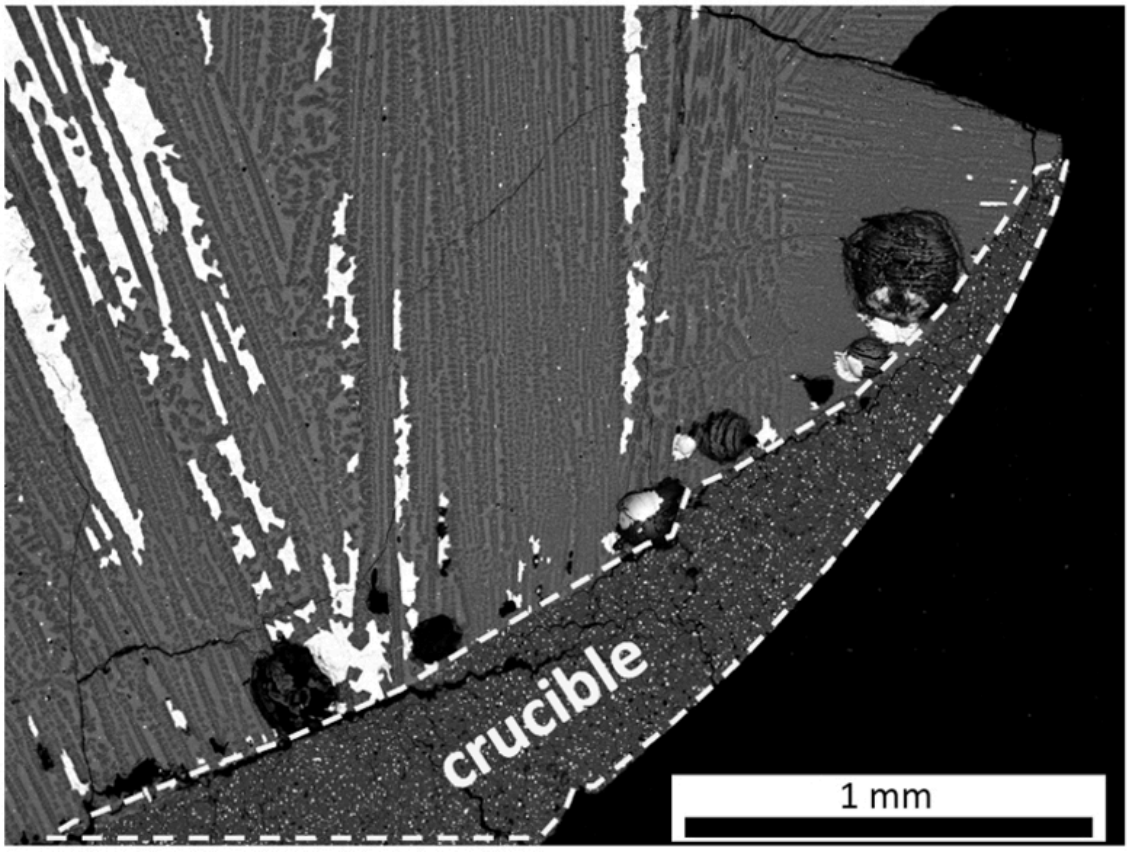

Figure 21. Platreef concentrate fired at 1480 °C. Matte (white phase) occluded in the porosity between the columnar enstatite crystals

Figure captions:

Figure 1. Schematic view of the black top with expected microstructures at (a) 1200 °C (b) 1300 °C (c) 1400 °C and (d) 1480 °C (the red line represents the temperature gradient). The black coloured phase in (a) to (d) represents a liquid phase.

Figure 2. Schematic view of the sealed capsule system (left) and capsules after welding (right)

Figure 3. Chemical compositions of the PGM concentrates (black squares) and maximum and minimum values found in the literature (dashed lines)

Figure 4. Liquid content in the concentrates as a function of temperature (predicted by FactSage®)

Figure 5. Linear shrinkage of the PGM concentrate samples after firing

Figure 6. UG–2 concentrate fired at 1480 °C: (a) bulk fired concentrate; (b) polished section showing a matte button at the bottom of the crucible

Figure 7. BEI of the UG–2 concentrate fired at 1480 °C showing the matte button–slag interface

Figure 8. Platreef concentrate fired at 1300 °C: (a) polished sections (OD = 50 mm) of the top and bottom sections; (b) bulk fired concentrate

Figure 9. BEI of Platreef concentrate fired at 1400 °C

Figure 10. BEI of Platreef concentrate fired at 1400 °C